Structural and electronic properties of epitaxial thin-layer Si_nGe_n superlattices

Sverre Froyen, D. M. Wood, and Alex Zunger
Solar Energy Research Institute, Golden, Colorado 80401
(Received 21 September 1987)

We examine theoretically structural and electronic properties of thin Si_nGe_n superlattices for $n=1$, 2, 4, and 6, grown on (001)-oriented substrates. The increased repeat distance along the growth direction leads to folding of conduction-band states to the Γ point of the superlattice Brillouin zone, resulting in a significant reduction in the minimum direct band gap. Transitions to these folded-in states have nonzero dipole matrix elements because of (i) atomic relaxation, leading to the accommodation of distinct Si—Si and Ge—Ge bond lengths and (ii) the superlattice ordering potential. Our calculations show that superlattices grown pseudomorphically on a Si substrate remain indirect-band-gap structures, with a minimum gap from Γ to Δ (near the X point) of the fcc Brillouin zone. We find, however, that increasing the lattice parameter a_s of the substrate will further reduce the direct band gap. For $a_s \gtrsim \bar{a}$, where $\bar{a}$ is the average of the lattice constants for Si and Ge, we predict a nearly direct band gap: For Si_6Ge_6 the indirect band gap for $a_s=\bar{a}$ is only ~ 0.01 eV smaller than the direct band gap. The lowest conduction-band states in this case are localized on the Si sublattice.

I. INTRODUCTION

One of the outstanding issues in semiconductor physics has been the hope to combine and manipulate Si and Ge to create a material that shares the advantageous properties of these semiconductors, yet has a *direct band gap* (and is capable of light emission). Attempts in this direction have been based on interstitial substitution,[1] application of pressure,[2-3] growth of *alloy* superlattices[4-8] $Si_n(Si_xGe_{1-x})_m$ on Si, and, more recently,[9,10] through growth of ultrathin *elemental* Si_nGe_n superlattices on a (001)-oriented Si substrate. Although theoretical studies on bulk solid solutions of Si_xGe_{1-x} alloys[11] are rather complete, until recently comparable studies on strained alloy superlattices of[12,13] $Si_n(Si_xGe_{1-x})_m$ or on strained elemental superlattices[14,15] Si_nGe_m have been performed on systems with rather long repeat periods (n,m). In such systems, simple approximations (perturbative expansion in terms of virtual-crystal orbitals,[12] the envelope-function approximation,[13] one-dimensional two-band models,[14] or the tight-binding approximation[15]) are applicable. The recent advent of *ultrathin* superlattices[9,10] and the observation of new, low-energy direct transitions[9] with no counterpart either in the bulk alloy[11] or in strained alloy superlattices,[4-8] have created the need for theoretical approaches capable of treating systems with atomic-scale repeat periods.

Although it has been observed[16] that the electronic charge density and potential approach their bulk values within one to two monolayers of an interface, the electronic states of ultrathin superlattices do not follow the simple scaling with layer thickness obeyed by ordinary thick superlattices. This is because the simple effective-mass or "particle-in-a-box" descriptions of quantum confined states break down in this case. The well width (proportional to the repeat distance) is no longer large compared with the width of the interface, so the effective potential is no longer piecewise constant along the repeat direction. Furthermore, for most states the band offsets are too small (given the narrow well width) to confine the states to a sublayer, and they will in general show three-dimensional delocalization over all sublattices. In this case it is more natural to consider the superlattice as a new type of compound semiconductor in its own right and to interpret its electronic properties in terms of distortions and band folding induced in the electronic structure of a disordered alloy of the same composition. A preliminary report has recently been published.[17] Related publications have also appeared[18,19] recently on the same subject.

This paper presents results of a density-functional study of Si_nGe_n superlattices for $n=1$, 2, 4, and 6. The method is discussed in Sec. II, Sec. III describes structural properties, including total energies as a function of layer thickness n, and electronic properties are discussed in Sec. IV. Section V discusses substrates other than Si.

II. METHOD

We use the momentum-space pseudopotential total-energy scheme[20] to determine structural energies and internal atomic forces and stress.[21] Atomic pseudopotentials are generated using a method described by Kerker.[22] Different, semirelativistic potentials for orbitals of s, p, and d symmetry are constructed to give the correct wave functions, energy levels, and excitation energies for a number of atomic configurations, including the positive and negative ions. The errors in the excitation energies are all smaller than 1 mRy, and usually much smaller.

Wave functions in the solid are expanded in a plane-wave basis, and the total energy, forces, and stress for a

given structure are computed as described in Refs. 20 and 21. The basis set contains plane waves up to a kinetic-energy cutoff of 12 Ry for total-energy calculations and up to 15 Ry for the (harder-to-converge) conduction-band energies. We estimate that the 15-Ry cutoff gives band energies accurate to 0.03 eV, with the exception of the s-like Γ'_{2c} state, where the error is 0.06 eV. This basis-set cutoff energy and the limited number of quadrature points used in Brillouin-zone integration[20] were found to lead to uncertainties in the total energy of the order of 2 mRy (30 meV). We find, however, that a small basis-set energy cutoff of 6 Ry is inadequate for calculating superlattice energy levels: not only are the errors large (e.g., for a Si_4Ge_4 superlattice on Ge, the energies obtained with 6 Ry cutoff are 0.54, 0.44, 1.1, and 1.1 eV higher than those obtained with 15 Ry cutoff for $X_c^{\parallel}$, $X_c^{\perp}$, L_c, and Γ'_{2c}, respectively), but these errors are also strongly state dependent, prohibiting a simple correction for the errors caused by insufficient convergence.

The calculations are carried out self-consistently[20] by evaluating the electronic charge density at the *equivalent* of six (10 for the $n=4$ superlattice) special points in the irreducible face-centered-cubic Brillouin zone. Exchange and correlation are treated within the local-density approximation[23] using the parametrization[24] of Perdew and Zunger of the electron-gas data of Ceperley and Alder.

The electron band energies we report are all calculated for superlattices in their theoretical equilibrium structure. The lattice parameters $a_{\parallel}$ parallel to the substrate are taken as the theoretical value for the substrate selected, assuming coherent, pseudomorphic growth.[25] All remaining structural degrees of freedom are determined through total-energy minimization. This includes relaxation of the $c/a_{\parallel}$ ratio and of the intracell interplanar spacings. In order to avoid costly first-principles scans of up to seven simultaneous structural parameters, structural relaxation was performed in three steps, as follows. First, bond-bending and bond-stretching force constants were determined from pseudopotential total-energy calculations for bulk Si, Ge, zinc-blende SiGe, and their epitaxial forms (i.e., fixing $a_{\parallel}$ and varying c). Next, preliminary superlattice interplanar spacings were found by energy minimization within the valence-force-field model,[26] using these force constants and bond lengths as input. Finally, the superlattice structure was refined (when necessary) using the full-pseudopotential total-energy method.[20,21] In this final phase, calculated forces and stress[27] were used to determine the minimum-energy configuration. We found that the valence force field with *ab initio* parameters gave interplanar spacings within 0.005 Å of the pseudopotential results. This changes the total energies by less than 0.07 meV per two atoms and the band energies by less than 30 meV.

The local-density approximation (LDA), with its well-known band-gap problem,[24] underestimates conduction-band energies. Fortunately, the lowest superlattice conduction bands derive only from states of Si and Ge around X and L (other states are displaced to higher energies because of strain and confinement effects; see Sec. IV). Our results can therefore be corrected approximately for the LDA errors by applying the average corrections needed to bring the LDA results for bulk Si and Ge into agreement with experiment. For the X_{1c} states of bulk Si and Ge, we find calculated LDA values lower than the observed[28(b)] results by 0.66 and 0.62 eV, respectively. We will, therefore, shift superlattice states evolving from X_{1c} upward by 0.64 ± 0.04 eV. For the L_{1c} states of Si and Ge, we find the LDA to underestimate the observed values by 0.58 and 0.46 eV, respectively. Since the superlattice states evolving from L_{1c} have approximately equal weights from Si and Ge (see Fig. 6 below), we will use the average correction of 0.52 ± 0.12 eV. We find the LDA to underestimate the Γ'_{2c} states by 0.86 and 0.58 eV for Si and Ge, respectively. Our error margin for Γ_c-derived superlattice states is therefore as large as ~0.3 eV. Fortunately, this state occurs at a very high energy (see Sec. IV E), so that this error does not affect our calculated band edges. In what follows we will report our local-density results directly, and apply the shifts above only in Sec. IV E 2, where comparison with experiment is made. Note that the local-density formalism produces good agreement with the measured deformation potentials (Sec. IV B), so that calculated band *shifts* caused by strain present in these strained-layer superlattices are expected to be accurate.

III. STRUCTURAL PROPERTIES OF STRAINED Si_nGe_n SUPERLATTICES

We calculate equilibrium lattice constants of 5.41 and 5.61 Å for pure Si and Ge, respectively. The experimental values[28(a)] are 5.430 and 5.657 Å.

Assuming the strain induced by the mismatch between Si and Ge lattice constants is accommodated elastically, the Si_nGe_n superlattices can grow pseudomorphically on a (001) Si substrate. The equilibrium lattice constant of Si_nGe_n (close to that for a disordered $Si_{0.5}Ge_{0.5}$ alloy) is about 2% larger than for pure Si. The superlattices therefore experience a biaxial strain of 2% in the [100] and [010] directions. The total strain energy can be reduced both by deforming the cell tetragonally and by relaxing the interplanar spacings in the [001] direction. The average relaxation makes the $c/a_{\parallel}$ ratio greater than 1 for a Si substrate, and smaller than one for a Ge substrate; this will be denoted as tetragonal distortion. We find for a Si substrate that all the superlattices (for $n=1$, 2, 4, and 6) deform by approximately the same amount: $c/a_{\parallel}=1.03\pm0.01$. The uncertainty is partially caused by numerical uncertainties in locating a shallow minimum in the total energy versus $c/a_{\parallel}$, and partly by our underestimating the lattice mismatch between bulk Si and Ge (since $c/a_{\parallel}$ is proportional to the lattice mismatch). Interplanar relaxations restore the interplanar spacings in the Si and Ge layers to very close to those for the pure constituents (Table I). For a Si substrate virtually all strain is taken up by the Ge layer. The spacing between adjacent planes α and β can be written as $d_{\alpha\beta}=(c/2n)(1+\varepsilon)$, where ε is the relaxation parameter (zero when atoms are unrelaxed). Our results show $\varepsilon\simeq-0.03$ for Si—Si bonds and $\varepsilon\simeq+0.03$ for Ge—Ge bonds. Hence, for a Si substrate, to within 0.01 Å, the

TABLE I. Interplanar distances (Å) for epitaxial Si_nGe_n superlattices ($n=2$, 4, and 6) grown pseudomorphically on a (001)-oriented substrate with substrate lattice parameter $a_{Si}=5.41$ Å, $\bar{a}=5.51$ Å, and $a_{Ge}=5.61$ Å, as obtained in valence-force-field geometry optimization using the *ab initio* force constants α(Si-Si)=47.207, α(Ge-Ge)=38.212, α(Si-Ge)=42.855, β(Si-Si-Si)=14.320, β(Ge-Ge-Ge)=12.387, β(Si-Ge-Si)=β(Ge-Si-Ge)=13.083, β(Si-Si-Ge)=13.674, and β(Si-Ge-Ge)=12.725, all given in N/m.

	R(Si—Si) Å			R(Si—Ge) Å			R(Ge—Ge) Å		
	a_{Si}	$\bar{a}$	a_{Ge}	a_{Si}	$\bar{a}$	a_{Ge}	a_{Si}	$\bar{a}$	a_{Ge}
$n=2$	1.3488	1.3303	1.3112	1.3926	1.3750	1.3568	1.4378	1.4220	1.4057
$n=4$	1.3524	1.3342	1.3154	1.3928	1.3752	1.3570	1.4344	1.4183	1.4017
	1.3505[a]	1.3321[a]	1.3132[a]				1.4364[a]	1.4205[a]	1.4040[a]
$n=6$	1.3521	1.3338	1.3150				1.4348	1.4187	1.4021
	1.3522[a]	1.3340[a]	1.3152[a]	1.3928	1.3752	1.3570	1.4346[a]	1.4185[a]	1.4019[a]
	1.3505[a]	1.3322[a]	1.3132[a]				1.4364[a]	1.4204[a]	1.4040[a]

[a]This distance occurs twice.

Si-Si interplanar distances are those of bulk Si (1.35 Å) and the Ge-Ge distances those of Ge grown epitaxially on Si (1.43 Å). The interlayer Si-Ge distance is close to the average of the other two. A small deviation from this rule is observed in the distances between the planes next to the Si-Ge interfaces (Table I). On the Ge side of the interface this distance is slightly larger than the other Ge-Ge distances; on the Si side it is smaller. The difference is small, less than 0.005 Å, but noticeable in both the $n=4$ and 6 superlattices.[29] The overshoot of the Ge—Ge bond length on the Ge side of the interface and of the Si—Si bond length on the Si side of the interface may reflect charge transfer across the interface: Since Ge is the more electronegative element, charge will flow from Si to Ge across the interface. The lattice expansion on the Ge side and the contraction on the Si side then act to restore the charge density toward the bulk value.

Our total-energy calculations permit assessment of superlattice stability. The *epitaxial* formation enthalpy δH is given[30] as the difference between the total energy of Si_nGe_n (where all of its structural parameters are relaxed for a fixed substrate lattice constant $a_\parallel$) relative to equivalent amounts of Si and Ge, also at $a_\parallel$ (and for which c is relaxed). We find, for Si as a substrate,

$$\delta H^{(n)}=0\pm 30 \text{ meV/[(Si-Ge) pair]}$$

for $n=1$, 2, 4, and 6 (to within 3 meV; the 30-meV error is the difference between the fitted and directly calculated Ge energy at equilibrium). If the total superlattice thickness exceeds h_c^{Ge}, the critical thickness for nucleation of misfit dislocations for Ge grown epitaxially on an (001) Si substrate, it is more appropriate to refer the formation enthalpy of the superlattice to equivalent amounts of (bulk) Si and *bulk* Ge. This gives

$$\Delta H^{(n)}=34\pm 30 \text{ meV/[(Si-Ge) pair]} .$$

Comparison of $\delta H^{(n)}$ with $\Delta H^{(n)}$ shows that the epitaxial superlattice is less unstable than the bulk superlattice, as previously noted.[30]

Previous calculations of the electronic structure of strained superlattices (e.g., Refs. 12–15, 18, and 19) have used tetragonally deformed unit cells ($c/a_\parallel \neq 1$), but have ignored energy-lowering interplanar relaxation within the tetragonal unit cell. We find (see Sec. IV E 2 below) that such displacements also sensitively control transition probabilities into folded-in conduction-band states.

IV. ELECTRONIC PROPERTIES

A. Conceptual model for formation of strained superlattice from bulk constituents

We are particularly interested in the direct versus indirect nature of the fundamental superlattice band gap and will therefore focus on the behavior of the low-energy conduction-band symmetry points Γ, X, and L and the Si conduction-band minimum at Δ_{min} (using the symmetry labels of the face-centered-cubic lattice). To gain insight into the origins and nature of these states and their evolution from the states of bulk Si and Ge, we will follow a stepwise conceptual process carrying bulk Si and bulk Ge into the final strained superlattice. We will use the case of a Si substrate and an equimolar superlattice (denoted Si_nGe_n/Si) to illustrate this process. Numerical results for other substrates are given in Sec. V.

In the *first step* we hydrostatically compress Ge from its equilibrium bulk lattice parameter (a_{Ge}) to that (a_{Si}) of the substrate on which it is grown. In the *second step* we allow its c axis to tetragonally deform to its equilibrium value for this substrate. Since the second superlattice component (Si) is unstrained when grown on a Si substrate, its electronic structure is computed at its (theoretical) bulk equilibrium lattice parameter a_{Si}. In the *third step* we combine bulk Si with tetragonally deformed Ge to form the strained epitaxial $Si_{0.5}Ge_{0.5}$ alloy (at its equilibrium value of $c/a_\parallel$). In this step we use the virtual-crystal approximation[31] to generate the band structure of the tetragonal alloy. In the *fourth* and final step we contrast the electronic structure of the $Si_{0.5}Ge_{0.5}$ *disordered* epitiaxial alloy with that of the *atomically ordered* and fully relaxed epitaxial Si_nGe_n superlattice. These two structures share the same composition and molar

volumes and differ only in the atomic ordering within the unit cell.

The structural parameters for each of the ordered compounds are determined by the same procedure outlined in Sec. III. For each step we compute self-consistently the electronic structure, using precisely equivalent basis sets and Brillouin-zone sampling points. Comparison of the results of the four steps will determine, respectively, the effects of (i) hydrostatic compression, (ii) tetragonal deformation, (iii) coexistence of chemically different constituents in the same cell, and (iv) superlattice ordering (with its attendant band-folding, band-coupling, and charge-transfer effects) on the electronic properties of the superlattice. The resulting band energies at high-symmetry points are depicted in Fig. 1.

B. Hydrostatic compression effects

Pure Ge can be grown pseudomorphically on[32] Si, provided that the strain resulting from the lattice mismatch can be accommodated elastically.[25] This results in a contraction of the (larger) in-plane Ge lattice parameter to match that of Si (a hydrostatic pressure effect), and an elongation of the lattice parameter in the perpendicular direction. In the first step we consider only the hydrostatic pressure effect. Comparing the electronic structure of bulk Ge (at a_{Ge}) of Fig. 1(a) with that of compressed Ge (at a_{Si}, but with $c/a_{\parallel}=1$), shown in Fig. 1(b), we see that those states which have positive deformation potentials[33] (Γ'_{2c} and L_c) have been displaced to higher energies, while the X_c state, with its smaller and *negative* deformation potential, is shifted to lower energies. (The calculated pressure deformation potentials[34] for Ge, using the same method employed here, are 11.6×10^{-6} eV/bar for Γ'_{2c}, 4.6×10^{-6} eV/bar for L_{1c}, and -1.4×10^{-6} eV/bar for X_{1c}, in good agreement with experiment.[33] The different deformation potentials of X_c and L_c result in an interchange in the character of the conduction-band minimum (X_c falls below L_c). Whereas in bulk Ge, we find Γ_c to be *below* X_c [by 0.4 eV, Fig. 1(a)], in compressed Ge Γ_c is *above* X_c by 0.7 eV. We will see in Sec. IV D that the strong upward displacement of the Ge Γ'_{2c} state described here, coupled with the yet higher energy position of the Si Γ'_{2c} state, will make this state inconsequential for low-energy transitions in the superlattice, leaving the Si and Ge X, Δ, and L states as the major candidates for superlattice band edges.

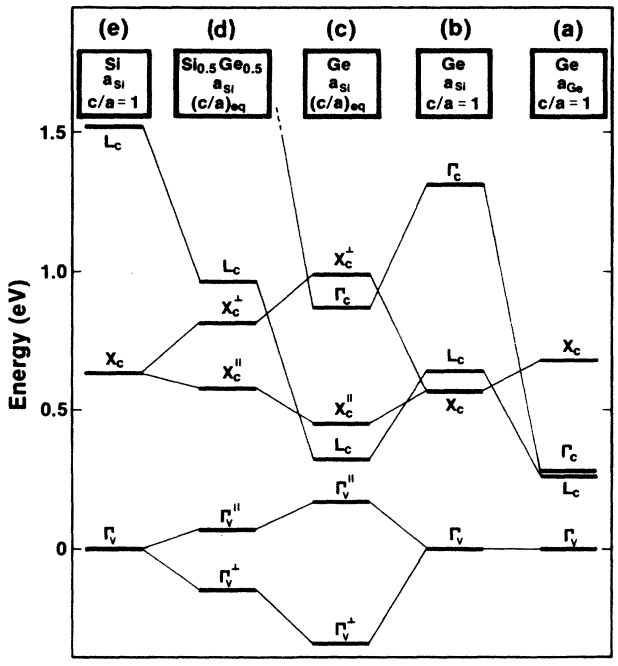

FIG. 1. Energy levels (in eV, relative to the average of the strain-split valence-band-maximum states) at Γ, X, and L of (a) bulk Ge ($a_{\mathrm{Ge}}=5.61$ Å) and (e) Si ($a_{\mathrm{Si}}=5.41$ Å), as well as (b) compressed and (c) tetragonally distorted Ge and (d) $Si_{0.5}Ge_{0.5}$ alloy.

C. Tetragonal deformation effects

Total-energy minimization calculations for epitaxial Ge on $a_{\parallel}=a_{\mathrm{Si}}$ show a tetragonal elongation of the perpendicular c axis to $c/a_{\parallel}=1.06$. The calculated electronic structure is depicted in Fig. 1(c). This biaxial compressive strain (along the [100] and [010] directions) splits the six equivalent fcc X_c conduction-band states into two equivalent $X_c^{\perp}$ states with their wave vector perpendicular to the substrate, and four equivalent $X_c^{\parallel}$ states. Each member retains the twofold degeneracy dictated by the point-group symmetry. For $c/a_{\parallel}>1$ (appropriate to a Si substrate) $X_c^{\perp}$ shifts to higher energies relative to $X_c^{\parallel}$ (we find for Ge a splitting of 0.5 eV). On the other hand, for $c/a_{\parallel}<1$ (appropriate, e.g., for Si on a Ge substrate), the order is reversed and $X_c^{\perp}$ is the lowest-energy state. The order of these states is crucial to the formation of a direct or indirect band gap. As will be evident in Sec. IV E 1, for a (001)-oriented superlattice, only the $X_c^{\perp}$ state folds into the center of the superlattice Brillouin zone. If $X_c^{\perp}$ is higher in energy than $X_c^{\parallel}$ (as is the case for a Si substrate), the system is likely to have an indirect band gap, whereas if $X_c^{\perp}$ is the lowest-energy state a direct band gap becomes possible. Wave vectors for the conduction states at L are oriented along the [111] direction and, therefore, these states remain unsplit by the biaxial strain appropriate to a (001)-oriented substrate. They shift uniformly to lower energies, leading to a near degeneracy with $X_c^{\parallel}$ [Fig. 1(c)].

The threefold-degenerate (in the absence of spin-orbit coupling) valence-band maximum splits into an upper, doubly degenerate $\Gamma_v^{\parallel}$ state and a singly degenerate $\Gamma_v^{\perp}$ state. Again, the order of these states depends on the tetragonal deformation: For Ge as the substrate (where $c/a_{\parallel}<1$), $\Gamma_v^{\parallel}$ is below $\Gamma_v^{\perp}$ (Fig. 10 below). Simple deformation-potential calculations[35–37] have been used in the past to estimate this splitting.

The combined upward displacement of $\Gamma_v^{\parallel}$ and downward displacement of L_c, both a consequence of epitaxial strain, reduce the indirect $\Gamma_v\rightarrow L_c$ band gap of tetragonally distorted Ge [Fig. 1(c)] relative to bulk Ge [Fig. 1(a)]. Furthermore, such deformations increase the direct

gap $\Gamma_v \rightarrow \Gamma_c'$. Hence, epitaxial strain alone makes Ge "less direct" relative to bulk Ge.

Suppose we were to form an interface between thick, tetragonally distorted Ge and a Si substrate. The relative energy levels would then be given by Figs. 1(e) (bulk Si) and 1(c) (tetragonal Ge), provided we align them to reflect the band offset between these systems, i.e., shift downwards the valence-band maximum of Si so that it is at an energy ΔE_v below the centroid of $\Gamma_v^{\parallel}$ and $\Gamma_v^{\perp}$ for tetragonally deformed Ge. As discussed at the end of Sec. II, the almost constant local-density error at the fcc L and X points of Si and Ge means that such an alignment using local-density values will correctly predict *relative* conduction-band energies. (Shifting conduction-band energies upward by 0.64 eV for X_c and by 0.52 eV for L_c will, moreover, give a realistic *absolute* band diagram.) Using our calculated value, $\Delta E = 0.50$ eV, for the average valence-band offset appropriate for Ge grown on Si (in good agreement with the offset, 0.54 eV, calculated by Van de Walle and Martin[16]), we find the results shown in Table II; a schematic picture is given in Figs. 2(b) and 2(c). Although in a thick Si_nGe_n superlattice the energies of the band-edge states will be those of the pure constituents adjusted for the relevant band offsets, in thin superlattices with a narrow well width d the energy is raised by quantum-confinement effects by[38] an amount $U = \pi^2\hbar^2/2m^*d^2$, where m^* is the appropriate effective mass. One expects that if $U > \Delta E$ the relevant state will extend over Si and Ge sublattices, while if $U < \Delta E$, the state will preferentially localize on that sublattice which has the lower (higher) potential energy for electrons (holes). Table II shows the calculated confinement energies U for $n=4$, using for d the sublayer thickness plus that of the interface layer. This can be used to obtain rough estimates of the nature of the Si_4Ge_4/Si states. The results show that we can expect the valence-band-maximum states to be delocalized (with slight localization on the Ge sublattice) and the $X_c^{\parallel}$, L_c, and Γ_c' states to be totally extended, while the $X^{\perp}$ state can be expected to localize on the Si sublattice. These simple expectations will be examined in Sec. IV E in light of our self-consistent superlattice calculations.

D. Forming the epitaxial disordered alloy

In the third step of our conceptual process of forming a Si_nGe_n superlattice epitaxially on Si, we consider mixing the states of bulk Si [Fig. 1(e)] with those of tetragonally deformed Ge [Fig. 1(c)] to form an epitaxial $Si_{0.5}Ge_{0.5}$ disordered alloy (not a superlattice). The electronic structure of this tetragonally deformed alloy is calculated in the virtual-crystal approximation,[31] taking the alloy pseudopotential as the average of those of Si and Ge. The epitaxial alloy is constrained to $a_{\parallel} = a_{Si}$, and we choose $c/a_{\parallel} = 1.03$ as the tetragonal elongation in the [001] direction. There are three noteworthy points about the alloy electronic structure: First, each alloy state has an energy very close to the average energy of its constituents, i.e., bulk Si [Fig. 1(e)] and tetragonally deformed Ge [Fig. 1(c)]. This near-averaging (small optical bowing parameter) is analogous to what is found in *bulk* Si_xGe_{1-x} alloy calculations.[11] This causes the low-energy L and Γ conduction-band states of tetragonally deformed Ge to shift up with respect to states at the X point, which now becomes the conduction-band minimum. (We shall see that this carries over to the superlattice. Hence the conduction-band minima of the superlattice will involve almost exclusively states of Si and Ge around X, for which local-density errors are nearly identical.) Second, since the tetragonal deformation for the alloy ($c/a_{\parallel} = 1.03$) is smaller than for Ge on Si ($c/a_{\parallel} = 1.06$), the $X_c^{\parallel}$-$X_c^{\perp}$ splitting is smaller in the alloy. Third, the strained alloy has a smaller gap then the bulk alloy: The $\Gamma_v^{\parallel} \rightarrow X_c^{\parallel}$ minimum gap of the *strained* alloy ($\sim$0.5 eV) is

TABLE II. Band offsets, ΔE (in eV, calculated here), effective masses m^* for the relevant states [Ref. 28(b)], and energy change $U = \pi^2\hbar^2/2m^*d^2$ (in eV) caused by confinement, relative to the well minimum. Results are given for an $n=4$ superlattice on a Si substrate. We use the value $d=7.0$ Å for the well width. For each state, we indicate in the last column the nature (localized or delocalized) of the wave function (in parentheses we indicate the sublattice on which the amplitude is larger).

Superlattice state	ΔE Magnitude	ΔE Minimum on	m^*	U	Expected nature of state
$\Gamma_v^{\parallel}$	0.7	Si	0.3[a]	2.6	delocalized (Ge)
$\Gamma_v^{\perp}$	0.2	Si	0.3	2.6	delocalized (Ge)
$X_c^{\perp}$	0.9	Si	0.98[b]	0.8	localized on Si
$X_c^{\parallel}$	0.3	Si	0.19[c]	4.0	delocalized
L_c	0.7	Ge	0.12[d]	6.4	delocalized
Γ_c'	2.1	Ge	0.04[e]	19	delocalized

[a]Ge hole mass at Γ.
[b]Si longitudinal-electron mass at X.
[c]Si transverse-electron mass at X.
[d][001] Ge electron mass at L.
[e]Ge electron mass at Γ_2'.

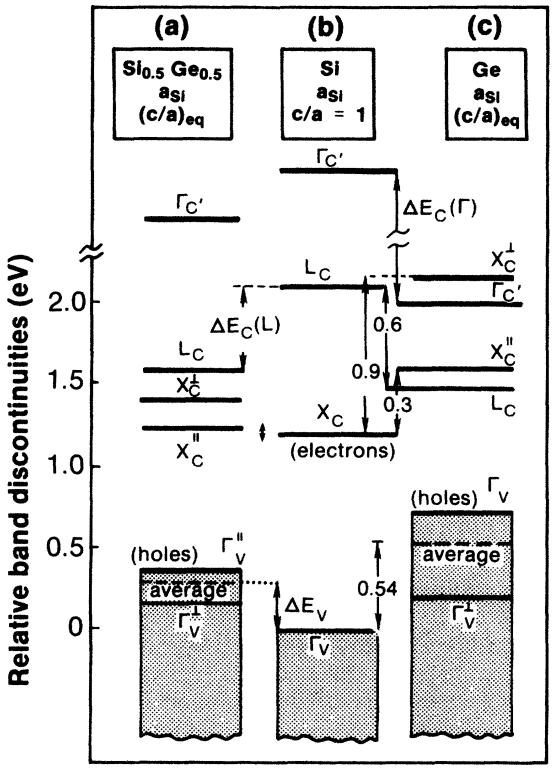

FIG. 2. Band-structure discontinuities of $Si_{0.5}Ge_{0.5}/Si$ [(a) and (b)] and Ge/Si [(b) and (c)]. The valence-band offsets ΔE_v are taken from Ref. 16. Relative conduction-band offsets are obtained from Fig. 1, by positioning the average energy of $\Gamma_v^{\parallel}$ and $\Gamma_v^{\perp}$ (denoted "average") of one material at a distance ΔE_v from the average of the other material. Due to the LDA error, the magnitude of the gap cannot be reliably given. Shifting the conduction band upwards by ~ 0.6 eV (see text), however, produces realistic X, Δ, and L gaps.

lower (by ~ 0.1 eV) than that of the *unstrained* alloy [0.64 eV: approximately the average of Figs. 1(a) and 1(e)].

If we were to form an interface between a thick $Si_{0.5}Ge_{0.5}$ alloy and a Si substrate, the relative energy levels would be those obtained by positioning Figs. 1(e) and 1(d) on an absolute energy scale. Using an approximate value for the valence-band offset of 0.27 eV (half the value appropriate for Ge on Si), we find the band diagram shown schematically in Figs. 2(a) and 2(b). It shows a small X_c-$X_c^{\parallel}$ conduction-band offset (with a shallow minimum on the Si side), but a larger valence-band offset (minimum on Si), predicting the formation of a predominantly two-dimensional hole gas. This corresponds to the situation realized in the $Si_n(Si_{0.8}Ge_{0.2})_m/Si$ system.[39] [Note, however, that if the substrate had a larger lattice constant, the conduction-band minimum would be lowered on the Si side, as was observed in the $Si_n(Si_{0.5}Ge_{0.5})_m/Si_{0.75}Ge_{0.25}$ system, where electron confinement to the Si layer was seen.[4]]

E. Ordering the disordered epitaxial alloy into a superlattice

1. *Folding symmetry and inequivalence of L and L' states*

The final step in the process of creating the strained superlattice from its bulk constituents involves the ordering of the atomic sites of the random $Si_{0.5}Ge_{0.5}/Si$ alloy, without changing the stoichiometry or the molar volumes.

When atoms are ordered into superlattice structures with their larger unit cells, the face-centered-cubic Brillouin zone (Fig. 3) of the alloy folds into smaller orthorhombic zones for even n (space group *Pmma*, point symmetry D_{2h}) and tetragonal zones for odd n (point group D_{2d}). Rather than use orthorhombic or tetragonal symmetry notation, we will retain the fcc labels (with an overbar added). This allows us to use a single, consistent set of labels and avoids a problem with the n-dependent fcc to orthorhombic or tetragonal mapping.

As a prelude to the discussion of the overall band gap of Si_nGe_n superlattices, we note that folding effects alone could conceivably make Si_nGe_n a direct-band-gap material. The disordered epitaxial $Si_{0.5}Ge_{0.5}$ alloy has a conduction-band minimum at a momentum k_c, between Γ and X. Simple geometry indicates that for $n=2/(1-k_c/k_X)$ (or an integer multiple), k_c will fold into $\bar{\Gamma}$. Taking $k_c \simeq 0.83 k_X$ (appropriate for Si) gives $n=12$. For an epitaxial Si_nGe_n superlattice, this estimate would be somewhat modified by strain and any ordering-induced change of k_c.

As noted in Sec. IV C, substrate-induced tetragonal distortion of a fcc structure splits the six equivalent X points into four equivalent $X^{\parallel}$ and two equivalent $X^{\perp}$ points [Fig. 1(d)]. In a superlattice, such a splitting will,

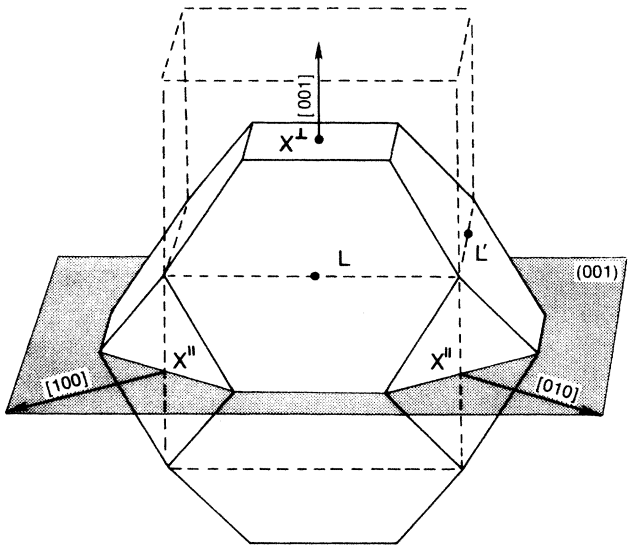

FIG. 3. Brillouin zone of the face-centered-cubic structure (solid lines) and the folded $n=2$ superlattice Brillouin zone (dashed lines), showing the nonfolding (L, $X^{\parallel}$, and L') as well as $\bar{\Gamma}$-folding ($X^{\perp}$) states.

in general, occur for Si_nGe_n (even or odd n), even in the absence of tetragonal distortion because of the chemical distinction between Si and Ge. In addition, in even-n superlattices the fourfold inversion axis along [001] is absent, rendering the [111] and [1$\bar{1}$1] L points inequivalent; the four $X^{\parallel}$ points remain equivalent. We choose the orientation of the superlattice such that the Si—Ge bonds are in the [111] and [$\bar{1}\,\bar{1}$ 1] directions and label the two inequivalent points $\bar{L}$ and $\bar{L}'$, directions and label the two inequivalent points $\bar{L}$ and $\bar{L}'$, respectively. (Odd-n superlattices have the $\bar{4}$ symmetry operation but lack inversion symmetry.) For an $n=2$ superlattice, the $X^{\perp}$ point folds into $\bar{\Gamma}$, and $X^{\parallel}$ points fold onto themselves. Since each of the $X^{\parallel}$ points was doubly degenerate before folding (because of the inversion symmetry), the folding of $X^{\parallel}$ in an $n=2$ superlattice doubles the degeneracy to four. Similarly, the L points ($\bar{L}$ and $\bar{L}'$) also fold onto themselves and become doubly degenerate.

To see how zone folding and band coupling change the character of the states, we have examined the virtual-crystal $Si_{0.5}Ge_{0.5}$ alloy in an $n=2$ superlattice cell, rather than in its primitive ($n=1$) cell. The probability densities for these states are shown in Fig. 4(b) in the ($\bar{1}$01) plane; in a (001) *superlattice* this plane will contain both types of atoms. Figures 4(a) and 4(c) show the corresponding results for pure Si and Ge, respectively, in the same unit cell. For Si, Ge, and $Si_{0.5}Ge_{0.5}$, in order to fix the phases and lift the degeneracies, we have added a tiny admixture of the superlattice "ordering potential" [$V(Si_2Ge_2)$-$V(Si_{0.5}Ge_{0.5})$]. In addition to the obvious periodicity (of repeat distance $c \simeq 1.03a_{\parallel}$) for the Si substrate) along the [001] superlattice growth direction, the ordering potential also creates an oscillating potential in the [110] direction with period $a_{\parallel}/\sqrt{2}$. Notice how this causes states with **k**-vector components along this direction ($\bar{X}^{\parallel}$ and $\bar{L}$) to acquire a periodicity of four monolayers in the [001] direction, while the $\bar{L}'$ states retain their double-layer periodicity. We shall see below (Sec. IV E 3) how this four-layer periodicity permits the wave functions to selectively localize in Si and Ge sublayers for certain n values.

For superlattices with $n>2$, more states will fold to the high-symmetry points. However, no additional, phase-changing degeneracies are created. The four-layer periodicity observed for $n=2$ is therefore preserved as the layer thickness increases.

The calculated energy levels for the $n=2$, 4, and 6 superlattices are shown in Fig. 5, where they are also compared with the virtual-crystal-approximation (VCA) alloy states. The corresponding wave-function amplitudes are plotted in Figs. 6(a)–6(c) for Si_2Ge_2, Si_4Ge_4, and Si_6Ge_6. We have chosen the degeneracy-weighted average of the three top valence bands at $\bar{\Gamma}$ as the zero of energy.

The uppermost valence bands for a Si substrate are all delocalized through both Si and Ge sublattices with a larger emphasis on the Ge sublattice. The lower, p_z-like state $\bar{\Gamma}_v^{\perp}$ is split from the upper $\bar{\Gamma}_v^{\parallel}$ states by the tetragonal deformation (a "crystal-field" splitting). The upper (p_x,p_y) pair, $\bar{\Gamma}_{v1}^{\parallel}$ and $\bar{\Gamma}_{v2}^{\parallel}$, is split because of the missing inversion axis.

While the total valence-band charge densities (lowest panels in Fig. 6) are rather similar in the disordered alloy and the ordered superlattices, substantial differences exist in the individual states. The conduction-band states fall naturally into two categories: the $\bar{\Gamma}$-folding states [Fig. 5(a)] $\bar{X}^{\perp}$ and $\bar{\Delta}^{\perp}$, where the lowest-energy states are localized on the Si sublattice, and the nonfolding states [Fig. 5(b)] $\bar{X}^{\parallel}$, $\bar{\Delta}^{\parallel}$, $\bar{L}$, and $\bar{L}'$, which have amplitude on both sublattices. We next discuss these two classes of states.

2. $\bar{\Gamma}$-folding on a Si substrate and new direct transitions

The $\bar{\Gamma}$-folding states behave as conventional quantum-confined states in two respects. First, except for the $n=2$ superlattice, they are confined to the Si sublattice, as can

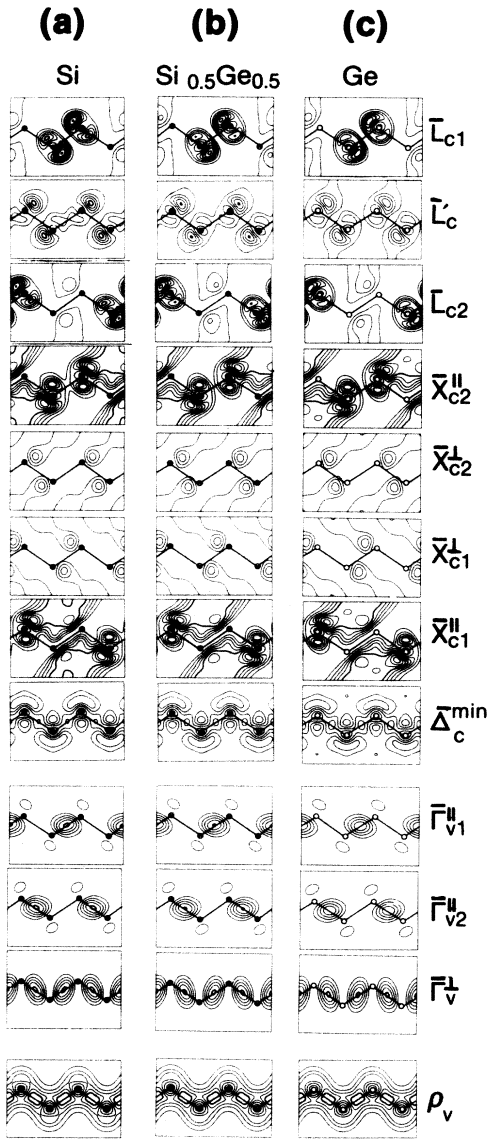

FIG. 4. Wave-function amplitude for Si [solid circles in (a)], epitaxial Ge/Si [open circles in (c)], and a virtual-crystal epitaxial $Si_{0.5}Ge_{0.5}$/Si alloy [crosses in (b)], calculated in a four-atom cell. A small potential perturbation has been introduced to infinitesimally lift the resulting X and L degeneracies.

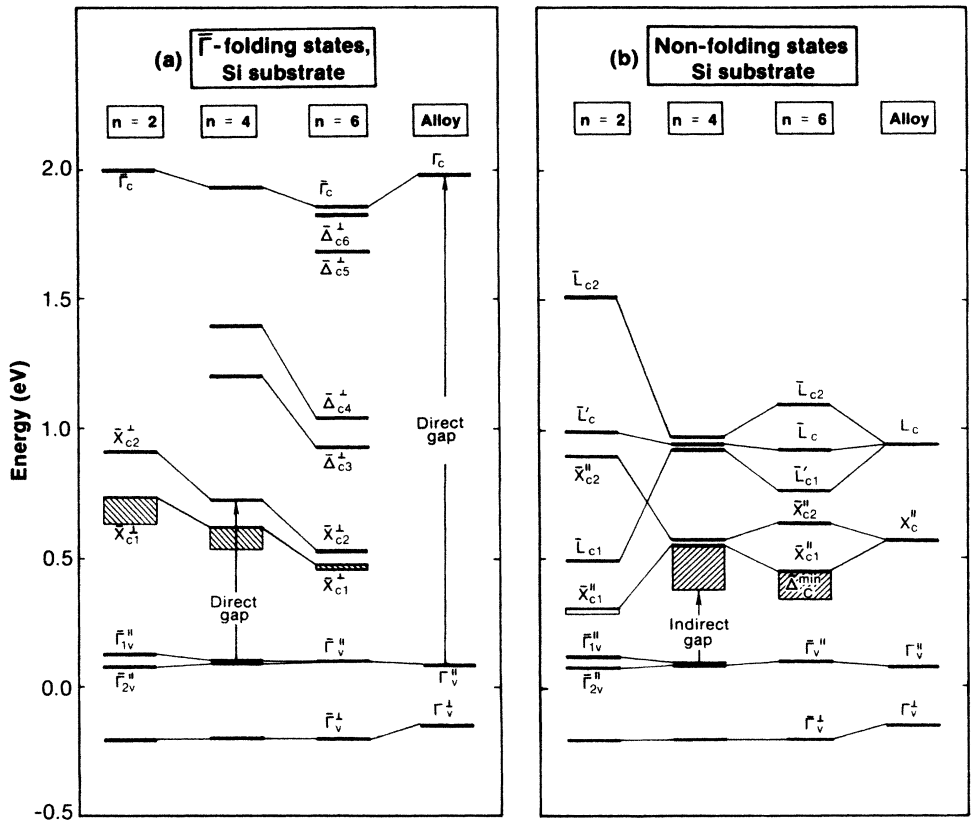

FIG. 5. Energy levels (in eV) of (a) quantum-confined longitudinal states and (b) extended transverse states of strained (001) Si_nGe_n superlattices grown on Si for $n=2$, 4, and 6 and for the random $Si_{0.5}Ge_{0.5}$ alloy on Si. Dashed boxed regions indicate the extent of downward dispersion of a band away from the symmetry point. The zero of energy is taken as the average of the top three valence states at Γ. Note in (a) that while the alloy has no direct transition below ~2 eV, the superlattice has six (for $n=6$) or four (for $n=4$) new direct transitions.

be seen by inspecting the $\bar{X}^{\perp}_{c1}$ and $\bar{X}^{\perp}_{c2}$ wave-function amplitudes in Fig. 6. Comparison with the corresponding wave-function amplitudes shown in Fig. 4 highlights the substantial segregation of charge in the superlattice (Fig. 6) relative to the alloy (Fig. 4). Second, the energy of the $\bar{\Gamma}$-folding states drops as the layer (well) thickness increases. The localization on a single sublattice of these $\bar{\Gamma}$-folding states (predicted also by simple models, see Table II) emphasizes the possibility of quantum confinement even in atomically thin superlattices. These $\bar{\Gamma}$-folding states are seen to occur in pairs, reflecting the original degeneracy at $X^{\perp}$.

For $n=4$ and 6 the additional states along Δ which fold into $\bar{\Gamma}$ still leave the conduction-band minimum along Δ (at $0.83k_X$) unfolded. This leads to a downward dispersion of the lowest-conduction-band state away from $\bar{\Gamma}$ in the [001] direction. The magnitude of this dispersion is indicated in Fig. 5 by the boxed region. For larger-n superlattices it is limited by Brillouin-zone edge effects and by the small dimension of the Brillouin zone in this direction.

Comparison of the direct transitions in the strained $Si_{0.5}Ge_{0.5}$/Si alloy with those of the strained superlattice [Fig. 5(a)] reveals a dramatic change: Whereas the lowest direct ($\Gamma^{\parallel}_v \rightarrow \Gamma_c$) transitions in the strained $Si_{0.5}Ge_{0.5}$ *alloy* appear above 1.9 eV, four new direct transitions appear in the Si_4Ge_4 *superlattice* below this energy. The occurrence in a superlattice of lower-energy pseudodirect-band-gap transitions even below the lowest indirect-band-gap transition of the bulk alloy of the same composition has also been reported in $(InAs)_n(GaAs)_n$ superlattices,[40] and in[41] $(GaAs)_n(AlAs)_n$ for $n>1$. (However, in these systems, at least one of the two compounds composing the superlattice has a direct band gap even in bulk form.)

Since the new low-energy conduction-band states are folded-in states, they would normally be expected to have small transition matrix elements with the upper valence-band states. (In the absence of superlattice ordering and atomic relaxations, such transitions carry *no* oscillator strength.) The transition matrix elements are, however, enhanced by the Si-Ge potential difference and by the different interplanar distances in the two sublayers (atomic relaxation, see Table I). As the layers become thicker the matrix elements must decrease and approach their vanishing bulk value for very thick layers. This is clearly seen in Table III, where the squares of the matrix elements are tabulated. Notice that in the $n=4$ superlattice the symmetry of the lower conduction bands is opposite that of the $n=2$ and 6 superlattices and all transitions to

the lowest-conduction-band state are dipole-forbidden. Figure 7 depicts the dipole-allowed transitions for parallel and perpendicular polarizations. Figure 8 shows the calculated matrix elements as a function of energy for direct transitions at $\bar{\Gamma}$. Since experimental[9] resolution is smaller than the $\bar{\Gamma}_{1v}^{\parallel}$-$\bar{\Gamma}_{2v}^{\parallel}$ splitting, the component transitions are not resolved.

We see that for parallel polarization [Fig. 8(b)] we expect three groups of transitions, denoted *A*, *B*, and *C*. Their energies (Table III), calculated in the local-density formalism for $n=4$, are 0.63, 1.11, and 1.84 eV, respectively. Correcting approximately for the local-density error (see Sec. II), this gives, for $n=4$,

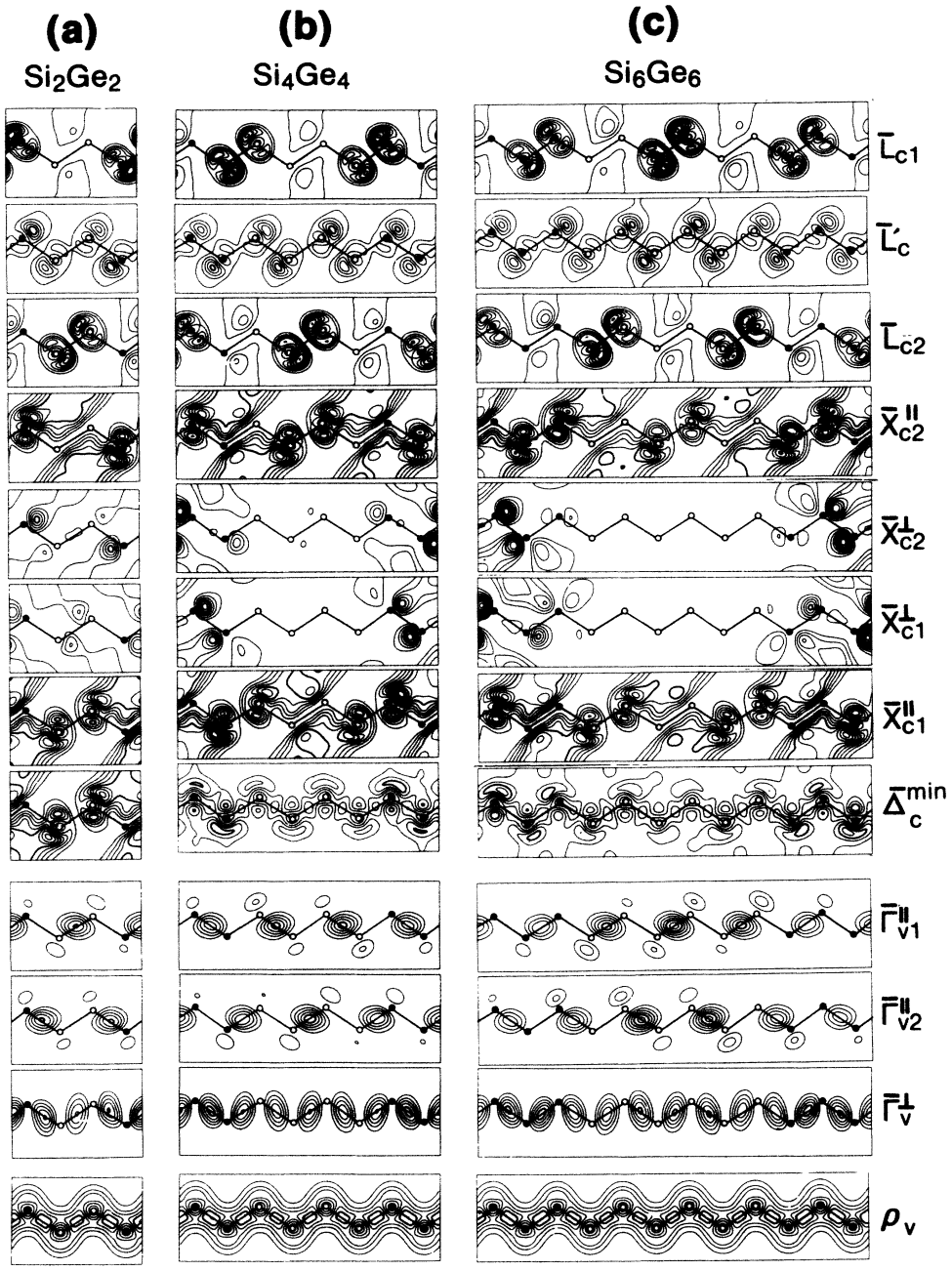

FIG. 6. Wave-function amplitude for states at $\bar{\Gamma}$, $\bar{X}$, $\bar{\Delta}_{\min}$, $\bar{L}'$, and $\bar{L}$, for (a) Si_2Ge_2/Si, (b) Si_4Ge_4/Si, and (c) Si_6Ge_6/Si. Results for $n=6$ are given in increasing order of energy; the energy order of $n=2$ and 4 is given in Fig. 5. Ge sites are denoted by open circles, Si sites by solid circles. The lowest panels give the total valence-band charge density. Note that while the lowest conduction bands ($\bar{\Delta}_c^{\min}$, $\bar{X}_{c1}^{\parallel}$) are delocalized, the next-highest conduction bands ($\bar{X}_{c1}^{\perp}$, $\bar{X}_{c2}^{\perp}$) are localized on the Si sublattice. Note further the four-layer periodicity of $\bar{L}_{c1}$ and $\bar{L}_{c2}$ for $n=4$ and 6.

TABLE III. Calculated dipole matrix elements $|\langle i|\mathbf{x}_\alpha|f\rangle|^2$ and transition energies ΔE in Si_nGe_n superlattices for $n=2$, 4, and 6 on a (001) Si substrate. (The values for a Ge substrate are given in parentheses for $n=4$.) $\langle i|$ is a valence-band state and $|f\rangle$ a conduction-band state as indicated; α is the direction of polarization. The notation for the states refers to Fig. 3. For a given valence band only one type of polarization gives nonzero matrix elements. The matrix elements have been normalized so that the strong, $\Gamma_{25v}\rightarrow\Gamma'_{2c}$-derived transition is unity. Energy differences are in eV.

		$\bar{\Gamma}^{\perp}_{v}(\alpha=\perp)$		$\bar{\Gamma}^{\parallel}_{2v}(\alpha=\parallel)$		$\bar{\Gamma}^{\parallel}_{1v}(\alpha=\parallel)$	
		$\lvert\langle\mathbf{x}_\alpha\rangle\rvert^2$	ΔE	$\lvert\langle\mathbf{x}_\alpha\rangle\rvert^2$	ΔE	$\lvert\langle\mathbf{x}_\alpha\rangle\rvert^2$	ΔE
$n=2$	$\bar{X}^{\perp}_{c1}$	0.21	0.93	1.28	0.65	0.07	0.61
	$\bar{X}^{\perp}_{c2}$	0	1.11	0	0.83	0	0.79
	$\bar{\Gamma}_c$	1	2.30	1	2.02	1	1.98
$n=4$	$\bar{X}^{\perp}_{c1}$	0	0.80 (0.24)	0	0.53 (0.43)	0	0.52 (0.41)
	$\bar{X}^{\perp}_{c2}$	0.02 (0.08)	0.91 (0.34)	0.04 (0.05)	0.63 (0.53)	$\simeq$0 (0.02)	0.63 (0.52)
	$\bar{\Delta}^{\perp}_{c3}$	0.04 (0.06)	1.39 (0.79)	0.12 (0.08)	1.11 (0.97)	$\simeq$0 ($\simeq$0)	1.11 (0.96)
	$\bar{\Delta}^{\perp}_{c4}$	0	1.58 (0.95)	0	1.30 (1.13)	0	1.30 (1.12)
	$\bar{\Gamma}_c$	1	2.12 (1.39)	1	1.84 (1.57)	1	1.84 (1.56)
$n=6$	$\bar{X}^{\perp}_{c1}$	0.01	0.67	0.11	0.37	$\simeq$0	0.37
	$\bar{X}^{\perp}_{c2}$	0	0.73	0	0.43	0	0.43
	$\bar{\Delta}^{\perp}_{c3}$	0	1.13	0	0.83	0	0.83
	$\bar{\Delta}^{\perp}_{c4}$	0.03	1.24	0.10	0.94	0.01	0.94
	$\bar{\Delta}^{\perp}_{c5}$	0.04	1.88	0.11	1.59	$\simeq$0	1.59
	$\bar{\Delta}^{\perp}_{c6}$	0	2.02	0	1.72	0	1.72
	$\bar{\Gamma}_c$	1	2.05	1	1.75	1	1.75

$$
\begin{aligned}
&(\bar{\Gamma}^{\parallel}_{1v},\bar{\Gamma}^{\parallel}_{2v})\rightarrow\bar{X}^{\perp}_{c2}\sim 1.27\pm0.04\ \text{eV}\ \ (A)\ ,\\
&(\bar{\Gamma}^{\parallel}_{1v},\bar{\Gamma}^{\parallel}_{2v})\rightarrow\bar{\Delta}^{\perp}_{c3}\sim 1.75\pm0.04\ \text{eV}\ \ (B)\ ,\\
&(\bar{\Gamma}^{\parallel}_{1v},\bar{\Gamma}^{\parallel}_{2v})\rightarrow\bar{\Gamma}_{c}\sim 2.6\pm0.3\ \text{eV}\ \ (C)\ .
\end{aligned}
\tag{1}
$$

We tentatively assign transition A to that observed[9] at 1.25 eV (with a linewidth of 0.13 eV), and the alloy-

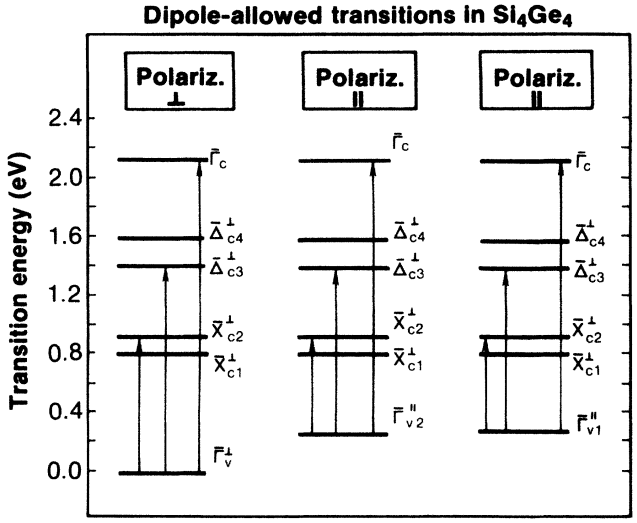

FIG. 7. Dipole-allowed transitions (neglecting spin-orbit coupling) for Si_4Ge_4/Si in different light polarizations. Note that transitions to the lowest folding ($\bar{X}^{\perp}_{c1}$) conduction band are forbidden.

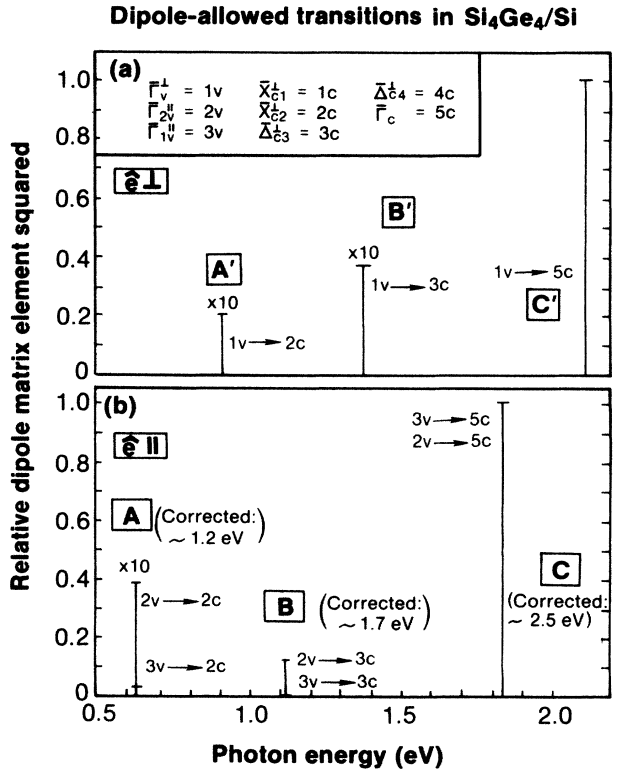

FIG. 8. Photon-energy dependent dipole transition elements for Si_4Ge_4/Si, showing three transitions (A', B', and C') for polarization $\hat{\mathbf{e}}\perp$ [in (a)] and three transitions for polarization $\hat{\mathbf{e}}\parallel$ [in (b)]. Values corrected approximately for the LDA error (a $\sim$0.6-eV shift) are given in parentheses.

derived ($\Gamma_v \rightarrow \Gamma_c$) transition C to that observed[9] at 2.31 eV (linewidth of 0.24 eV). The transition observed[9] at 0.76 eV is not a direct-band gap transition according to our calculation. It could correspond to the *indirect* $\bar{\Gamma}_v^{\parallel} \rightarrow \bar{\Delta}_c^{\min}$ transition [0.28 eV from Fig. 5(b), or 0.92±0.04 eV after correcting for the LDA error]. Transition B was not reported in the experimental study.[9]

In their tight-binding study, Brey and Tejedor[19] find for $n=4$ transition A at 1.1–1.2 eV, transitions B at 1.5–1.6 eV, and transition C at ~2.2 eV. People and Jackson[18] apparently do not find a transition of type B, possibly because they have assumed a single (rather than a double) folding in the $n=4$ superlattice.

Our calculation does not include spin-orbit (SO) coupling; qualitative effects can, however, be assessed from the quasicubic model of Hopfield:[42] (i) dipole-forbidden transitions in the absence of SO couplings (Table III) can become weakly allowed by mixing states belonging to the same inversion parity. (ii) Transition energies from $\bar{\Gamma}_{\frac{1}{2}v}^{\parallel}$ to the conduction band are reduced by $\sim\Delta_0/3$, where Δ_0 is the spin-orbit splitting of the superlattice valence-band maximum (approximately the average of $\Delta_0(\text{Ge})=0.3$ eV,[43(a)] and $\Delta_0(\text{Si})=0.03$ eV [Ref. 43(b)]). This reduces the corresponding values of Eq. (1), and the indirect $\bar{\Gamma}_v^{\parallel} \rightarrow \bar{\Delta}_c^{\min}$ gap by $\Delta_0/3=0.05$ eV, bringing them into closer accord with experiment. (iii) The $\bar{\Gamma}_v^{\perp}$-$\bar{\Gamma}_v^{\parallel}$ crystal-field splitting would increase by $\sim\Delta_0/2=0.075$ eV.

3. *Nonfolding states on a Si substrate*

Figure 5(b) shows, for a Si substrate, the variation of the indirect-band-gap states with the superlattice period n. The nonfolding $\bar{X}^{\parallel}$, $\bar{L}$, and $\bar{L}'$ states are extended on both Si and Ge sublayers [Fig. 5(b)]. The fourfold degeneracy of the alloy $X_c^{\parallel}$ state is split by the superlattice potential into upper and lower pairs.

The doubly degenerate L point is split at $\bar{L}$ into $\bar{L}_{c1}$ and $\bar{L}_{c2}$ [Fig. 5(b)] but remains degenerate at $\bar{L}'$. Figure 5(b) shows that the splitting of the $\bar{L}_{c1}$ and $\bar{L}_{c2}$ states oscillates with n, exhibiting a large energy difference for $n=2$ and 6 and near degeneracy for $n=4$. A similar effect was recently predicted[44] for $(\text{GaAs})_m(\text{AlAs})_m$ superlattices, showing large (small) $\bar{L}_{c1}$-$\bar{L}_{c2}$ splitting for m odd (even). This variation with n in the magnitude of the splitting is simply a measure of the commensurability of the superlattice period with the period of the wave functions. In the alloy we saw that the underlying period of the wave functions was four monolayers (Fig. 4). Thus the lattice is in perfect registry with the wave function in the $n=2$ superlattice and the states are able to fully sample the difference between the Si and Ge potentials, resulting in a maximum splitting. For $n=4$ the states are forced to sample both sublattices equally and the splitting is close to zero [Fig. 5(b)]. For $n=6$ each wave function can place $\frac{2}{3}$ of its weight on one sublattice and $\frac{1}{3}$ on the other, giving $\frac{1}{3}$ of the splitting of the $n=2$ superlattice [Fig. 5(b)]. In general, the splitting is zero for n a multiple of 4; for other n the wave function has relative amplitudes of $2/n$ and $(n-2)/n$ on the two sublattices, leading to a splitting $2/n$ times that for $n=2$. Because of their delocalized nature, the average of the states changes only slightly with n, although for sufficiently thick layers the states will localize and the energy will drop. This nonmonotonic behavior of the superlattice $\bar{L}$- and $\bar{X}$-point conduction-band energies [Fig. 5(b)], coupled with the small variations with n we find for the $\bar{L}$- and $\bar{X}$-point valence-band states, suggests that the energy of direct $\bar{X}_v \rightarrow \bar{X}_c$ and $\bar{L}_v \rightarrow \bar{L}_c$ transitions should be nonmonotonic as a function of n. Our calculations (uncorrected for LDA errors) predict splittings $\bar{X}_c$-$\bar{X}_v$ of 3.43, 3.73, and 3.64 eV, and $\bar{L}_c$-$\bar{L}_v$ splittings of 1.43, 1.93, and 1.78 eV, respectively, for $n=2$, 4, and 6. Experimental testing of this prediction is lacking.

Comparison of the wave-function amplitudes for the few lowest-conduction-band states of the superlattice (Fig. 6) reveals an interesting situation where the *lowest*-energy states ($\bar{\Delta}_c^{\min}$ and $\bar{X}_{c1}^{\parallel}$) are *delocalized*, while *higher*-energy states $\bar{X}_{c1}^{\perp}$ and $\bar{X}_{c2}^{\perp}$ are *localized* (the opposite of what might be expected from a single-well–type Kronig-Penney model[38]). This is understandable, however, in terms of the different barrier heights (Fig. 2 and Table II) and appropriate effective masses of the strain-split $X_c^{\perp}$ and $X_c^{\parallel}$ bands, discussed in Sec. IV C.

V. OTHER SUBSTRATES

In all the superlattices described so far, the indirect states at $\bar{X}^{\parallel}$ are well below the $\bar{\Gamma}$-folding $\bar{X}_c^{\perp}$ states. This makes all of these superlattices indirect-band-gap systems. The origin of this situation is the tetragonal deformation imposed by the substrate. If the substrate lattice constant is increased, the $c/a_{\parallel}$ ratio will decrease, and the order of $\bar{X}^{\perp}$ and $\bar{X}^{\parallel}$ is reversed (Fig. 9). To test this hypothesis, we performed two additional calculations, one for an $n=4$ superlattice with an in-plane lattice constant $a_{\parallel}=\bar{a}$, the average of Si and Ge (appropriate for a superlattice grown on a $Si_{0.5}Ge_{0.5}$ alloy or for a free-standing superlattice), and the other for an $n=4$ superlat-

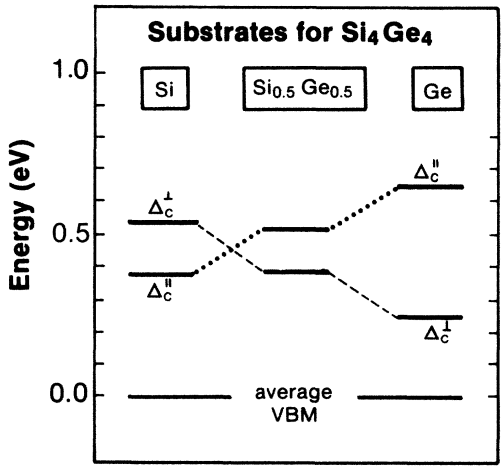

FIG. 9. Change in level ordering between $\bar{\Gamma}$-folding ($\Delta_c^{\perp}$) and nonfolding ($\Delta_c^{\parallel}$) states as a function of substrate lattice constant, for Si, $Si_{0.5}Ge_{0.5}$, and Ge substrates.

tice on Ge. Results for these calculations are shown in Figs. 9 and 10.

We observe that as the substrate lattice constant increases (i.e., the $c/a_{\parallel}$ ratio decreases) the $\bar{X}_c^{\parallel}$ (or $\Delta_c^{\parallel}$) states shift up in energy with respect to the $\bar{\Gamma}$-folding states at $\bar{X}^{\perp}$ (or $\bar{\Delta}^{\perp}$) (Fig. 9). For $a_{\parallel}=\bar{a}$ this shift is already sufficient to place the previous minimum at $\bar{\Delta}_c^{\min}$ close to $\bar{X}^{\parallel}$, above the lowest conduction band at $\bar{X}_{c1}^{\perp}$. The superlattice remains indirect, however, because of the 0.1-eV downward dispersion away from $\bar{\Gamma}$ in the [001] direction. The magnitude of this dispersion can be reduced by increasing n. For $n=6$ it is already only 0.01 eV and for superlattices with $n\sim 10-12$ it should vanish completely as the minimum of the alloy's first conduction band at $0.83k_X$ folds to $\bar{\Gamma}$. The growth of Si_nGe_n on an $x=0.5$ alloy substrate should be facilitated by the smaller strain in the layers (2%) relative to the situation with a Si substrate (4% strain). An added advantage is that, since the average strain for $Si_nGe_n/Si_{0.5}Ge_{0.5}$ is zero, there is no limit on the total thickness of the superlattice; the growth of optical thicknesses should be possible. Notice also from Fig. 10 that increasing the substrate lattice parameter leads to an interchange in the order of the $\bar{\Gamma}_v^{\perp}$ and $\bar{\Gamma}_v^{\parallel}$ valence-band states and, hence, to a reversal of the sign of the crystal-field splitting.

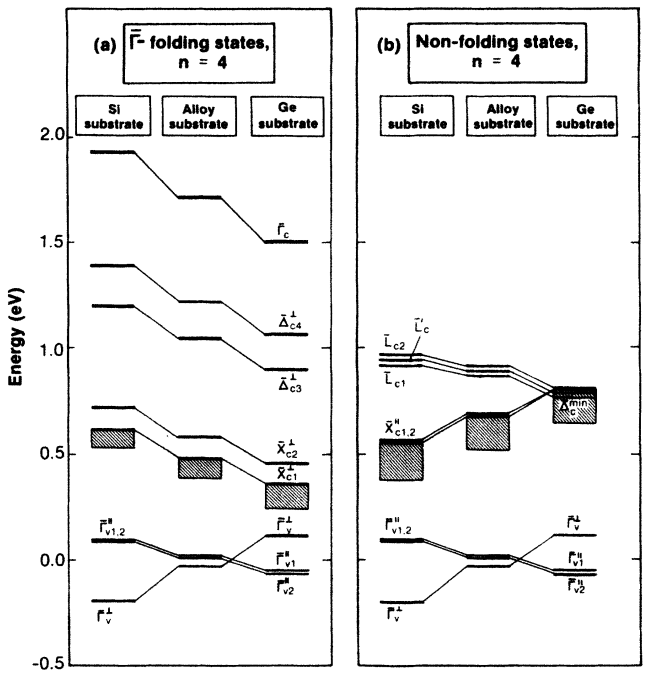

FIG. 10. Energy levels (in eV) of (a) quantum-confined longitudinal states and (b) extended transverse states of a Si_4Ge_4 superlattice matched epitaxially to Si, a $Si_{0.5}Ge_{0.5}$ alloy, and Ge substrates. Dashed regions indicate the extent of downward dispersion of a band from the symmetry point. The zero of energy is taken as the average of the $\bar{\Gamma}_{v1}^{\parallel}$, $\bar{\Gamma}_{v2}^{\parallel}$, and $\bar{\Gamma}_v^{\perp}$ states. Note the change in order of the crystal-field-split states $\bar{\Gamma}_{v1,2}^{\parallel}$ and $\bar{\Gamma}_v^{\perp}$ as the substrate lattice constant is changed.

VI. DISCUSSION AND CONCLUSIONS

We summarize the essential effects of strain and confinement on the electronic structure of strained Si_nGe_n in Fig. 11, depicting the potential wells, energy levels, and wave functions of the near-edge states for Si_4Ge_4 on a Si substrate [11(a)] and a Ge substrate [11(b)].

First, if quantum-confinement effects could be neglected (e.g., for a thick superlattice), the energy levels near the band edges would be given simply by the bulk band edges. The thick solid horizontal lines of Fig. 11 indicate these potential energies. These show that in the presence of strain the band offsets can be radically different for the $\perp$ and $\parallel$ states. For a Si substrate, the valence-band maximum ($\bar{\Gamma}_v^{\parallel}$) is Ge-like, while the conduction-band minimum ($\bar{X}_c^{\parallel}$) is on the Si sublattice; hence the system is a "type-II" superlattice. For a Ge substrate [Fig. 11(b)], the altered sign of the strain causes the $\bar{\Gamma}_v^{\perp}$ band edge to be *above* the $\bar{\Gamma}_v^{\parallel}$ band edge, and, likewise, the conduction-band edges for $\bar{X}_c^{\perp}$ and $\bar{X}_c^{\parallel}$ appear in a reverse order relative to the Si substrate, with $\bar{X}_c^{\perp}$ below $\bar{X}_c^{\parallel}$. Again, the system is a "type-II" superlattice, with the valence-band maximum ($\bar{\Gamma}_v^{\perp}$) on Ge and the conduction-band minimum ($\bar{X}_c^{\perp}$) on Si.

When the superlattice is made thin, the energy levels are no longer given by the bulk band edges. The dashed horizontal lines in Fig. 11 show the calculated energy levels ($n=4$) within these potential wells and the shaded regions indicate the weight of the wave functions on the sublattice. Wave-function amplitudes averaged over the (001) plane are shown in Fig. 12. For the Si substrate, we find that the energy level $\bar{\Gamma}_v^{\parallel}$ is 0.34 eV lower than the bulk $\Gamma_v^{\parallel}$ level. Despite the large barrier height, this state is delocalized on both sublattices (with a somewhat larger amplitude on the Ge side). The conduction-band minimum is indirect at $\bar{\Delta}_c^{\min}$; its wave-function amplitude is delocalized on both sublattices, with a slightly larger amplitude on the Si side. Hence, while for *large repeat periods* Si_nGe_n/Si would be judged to be a strong "type-II superlattice," for *small repeat periods* we find only a weak "type-II" behavior, with substantial delocalization on both sublattices.

For a thin superlattice grown on Ge [Fig. 11(b)], we find that although the wave-function amplitudes are very similar to the corresponding states on an Si substrate [e.g., compare $\bar{\Gamma}_v^{\perp}$ or $\bar{X}_c^{\perp}$ in Figs. 11(a) and 11(b)], the *order* of these states is changed. The valence-band maximum is at $\bar{\Gamma}_v^{\perp}$ (delocalized with a slightly greater emphasis on the Si sublattice) and the conduction-band minimum is close to $\bar{X}_c^{\perp}$ (strongly localized on the Si sublattice). The gap separating these states (~ 0.86 eV) is the minimum direct band gap, slightly larger than the indirect band gap. Quantum-confinement effects lead to the lowering of $\bar{\Gamma}_v^{\perp}$ relative to the bulk value Γ(Ge) and to the increase of $\bar{X}_c^{\perp}$ relative to the bulk value $X^{\perp}$(Si). Hence, the direct band gap $\bar{\Gamma}_v^{\perp}\rightarrow\bar{X}_c^{\perp}$ in the thin superlattice is larger than expected from the thick superlattice ($E_g^D\sim 0.5$ eV). The system is a weak "type-I" superlattice.

Our first-principles calculations of the evolution of the

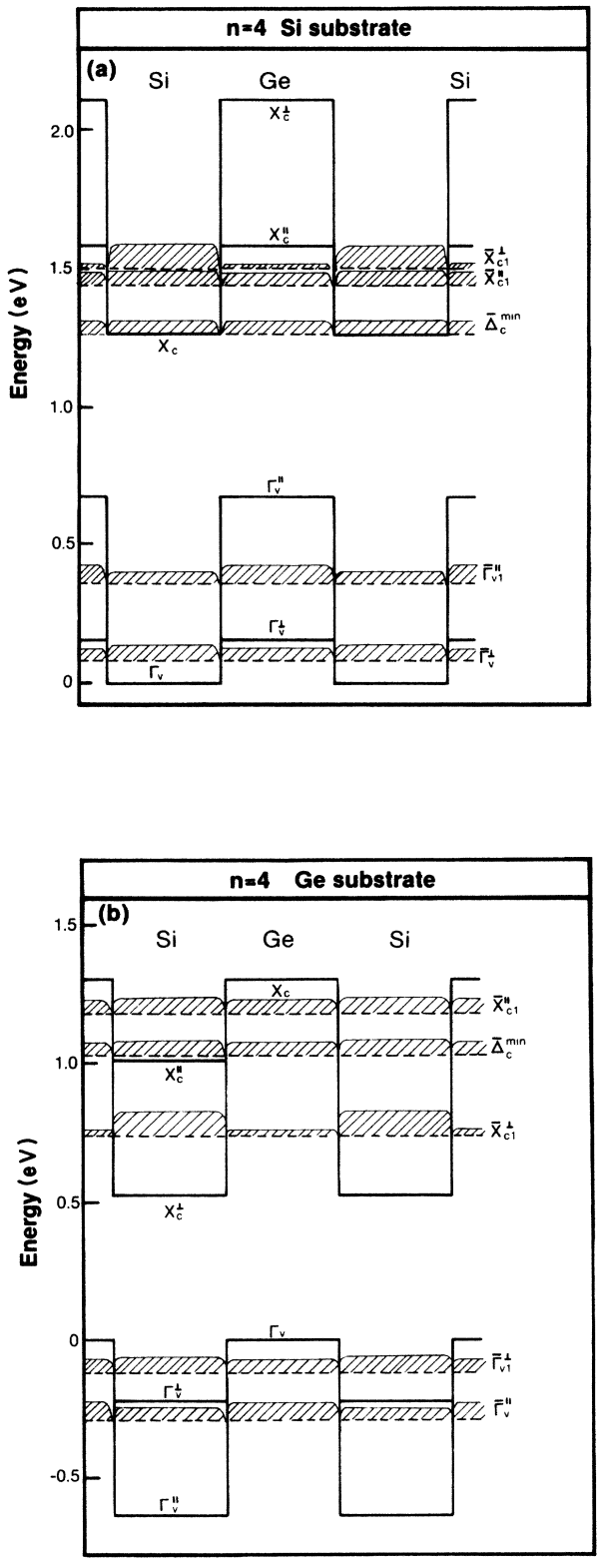

FIG. 11. Calculated band offsets for the Si-Ge interface (thick solid lines) and the corresponding Si_4Ge_4 superlattice energy levels (dashed line) for selected states. Results are shown for (a) Si and (b) Ge substrates. The shaded regions indicate the weight of the wave functions on the Si and Ge sublattices.

states of the strained superlattice from those of its bulk constituents reveal the following trends.

(i) Compressing Ge to the equilibrium volume of Si sharply raises its L_c and Γ_c conduction bands, while lowering X_c and making it the conduction-band minimum.

(ii) Tetragonally deforming Ge ($c/a_{\parallel} > 1$) leads to a splitting of the sixfold degeneracy of the X_c valleys into a lower-energy $X_c^{\parallel}$ state and a higher-energy $X_c^{\perp}$ state.

(iii) The states of an epitaxial tetragonally deformed $Si_{0.5}Ge_{0.5}$/Si alloy can be well described as an average of the corresponding states of bulk Si and tetragonally distorted Ge. This displaces the Ge Γ_c and L_c states to high energies, effectively removing them from the near-edge region. This alloy has a $\Gamma_v \rightarrow X_c^{\parallel}$ indirect band gap, and no direct transition below ~ 2 eV.

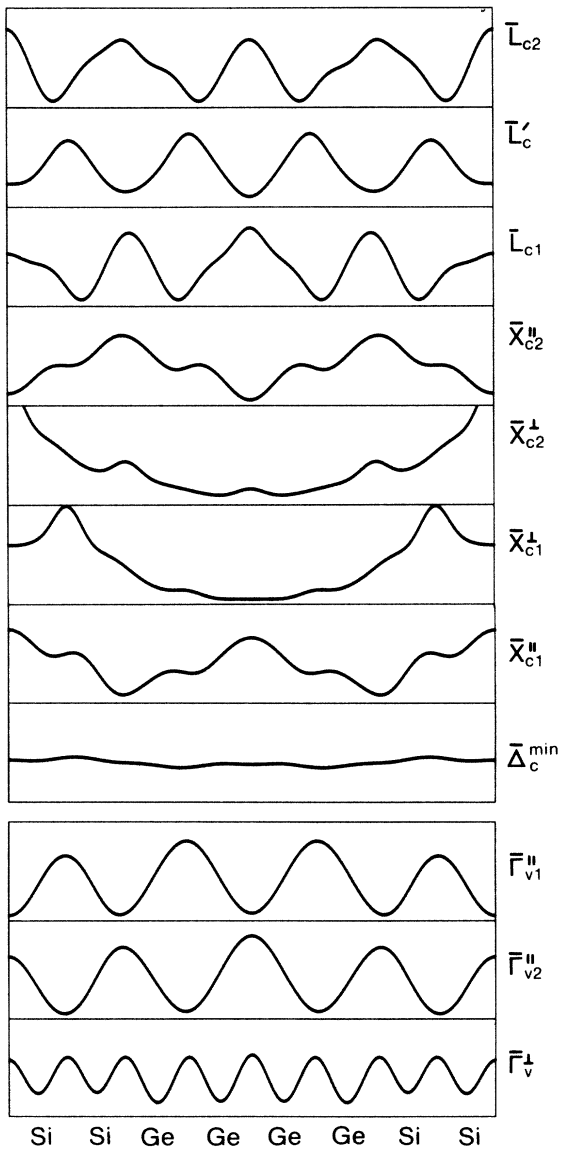

FIG. 12. (001) planar-averaged wave functions for selected states in the Si_4Ge_4 superlattice on a Si substrate.

(iv) Organizing the atoms of the epitaxial $Si_{0.5}Ge_{0.5}$/Si random alloy into the ordered pattern of a Si_nGe_n/Si superlattice leads to the usual band folding and band coupling. Since the higher-energy state [see (ii) above] $X^{\perp}$ folds into $\bar{\Gamma}$ but $X^{\parallel}$ does not, such superlattices grown on a Si substrate have an indirect band gap.

(v) Nevertheless, folding creates pseudodirect-band-gap states of $\bar{X}_c^{\perp}$ type which give rise to new direct transitions below 2 eV, a region in which no direct transitions exist in the equivalent disordered alloy. While small, the oscillator strengths of these transitions are nonetheless finite because of hybridization and atomic relaxations. Two of these transition energies (A and C at 1.27 and 2.6 eV, respectively) compare well with the observed transitions (after approximately correcting for the LDA error). The intermediate transition (B, at 1.75 eV) has no counterpart in the observed spectra. The lowest observed transition at 0.76 eV is not a pseudodirect transition; it is likely that this is the indirect transition $\bar{\Gamma}_v^{\parallel} \rightarrow \bar{\Delta}_c^{\min}$.

(vi) Whereas the lowest-energy folded states $\bar{X}_{c1}^{\perp}$ and $\bar{X}_{c2}^{\perp}$ are localized on the Si sublattice, the yet lower indirect-band-gap states ($\bar{\Delta}_c^{\min}$, $\bar{X}_{c1}^{\parallel}$) are delocalized on both the Si and Ge sublattices. This results from strain-induced changes in conduction-band offsets and differing effective masses. The valence band is similarly extended on both sublattices. Si_nGe_n/Si is hence a "type-II" superlattice, with holes on Si and Ge (but more on Ge) and electrons on the Si sublattice.

(vii) The absence of a fourfold inversion axis along [001] for even-n superlattices creates two inequivalent L points ($\bar{L}$ and $\bar{L}'$). The $\bar{L}_c$ as well as the $\bar{X}_c^{\parallel}$ states exhibit a periodicity of four monolayers, whereas the $\bar{L}_c'$ states retain their single-layer periodicity. Commensurability conditions of the four-layer periodicity of $\bar{L}_c$ and $\bar{X}_c^{\parallel}$ with the thickness n of the superlattice leads to an oscillating dependence of their energies on n. This should be observable in direct, $\bar{L}_v \rightarrow \bar{L}_c$, and $\bar{X}_v^{\parallel} \rightarrow \bar{X}_c^{\parallel}$ transitions.

(viii) The main reason for the occurrence of a low-lying indirect band gap in Si_nGe_n/Si was found to be the positive superlattice tetragonal deformation ($c/a_{\parallel} > 1$). Calculations for substrates with a larger lattice parameter (e.g., a $Si_{0.5}Ge_{0.5}$ alloy) show smaller tetragonal deformations and consequently a reversal of the order of the folding $X_c^{\perp}$ state with the nonfolding $X_c^{\parallel}$ state. We predict that $Si_6Ge_6/Si_{0.5}Ge_{0.5}$ will show a nearly direct band gap (only $\sim$0.01 eV above the indirect band gap).

[1] H. W. A. Rompa, M. F. H. Schuurmans, and F. Williams, Phys. Rev. Lett. **52**, 675 (1984); A. E. Carlsson, A. Zunger, and D. M. Wood, Phys. Rev. B **32**, 1386 (1985); D. M. Wood, A. Zunger, and R. deGroot, *ibid.* **31**, 2570 (1985); S.-H. Wei and A. Zunger, Phys. Rev. Lett. **56**, 528 (1986).

[2] Y. X. Zhao, F. Buehler, J. R. Sites, and I. Spain, Solid State Commun. **59**, 679 (1986); J. Z. Hu, L. D. Merkle, C. S. Menoni, and I. Spain, Phys. Rev. B **34**, 4679 (1986); J. M. Mignot, G. Chouteau, and G. Martinzez, *ibid.* **34**, 3150 (1986); S. J. Duclos, Y. K. Vohra, and A. L. Ruoff, Phys. Rev. Lett. **58**, 775 (1987); C. S. Menoni, J. Z. Hu, and I. L. Spain, Phys. Rev. B **34**, 362 (1986).

[3] K. J. Chang and M. L. Cohen, Phys. Rev. B **34**, 8581 (1986); **31**, 7819 (1985); H. Tanaka and K. Shindo, J. Phys. Soc. Jpn. **52**, 572 (1983); R. Biswas, R. M. Martin, R. J. Needs and O. H. Nielsen, Phys. Rev. B **35**, 9559 (1987).

[4] H. Jorke, H. J. Herzog, E. Kasper, and H. Kibble, J. Cryst. Growth **81**, 440 (1987); E. Kasper, H. J. Herzog, H. Jorke, and G. Abstreiter, Superlatt. Microstruct. **3**, 141 (1987); G. Abstreiter, H. Brugger, T. Wolf, H. Jorke, and H. J. Herzog, Phys. Rev. Lett. **54**, 2441 (1985).

[5] D. C. Houghton, D. J. Lockwood, M. W. C. Dharma-Wardana, E. W. Fenton, J. M. Baribeau, and M. W. Denhoff, J. Cryst. Growth **81**, 434 (1987).

[6] H. M. Manasevit, I. S. Gergis, and A. B. Jones, Appl. Phys. Lett. **41**, 464 (1982); J. Electron. Mater. **12**, 637 (1983).

[7] A. T. Fiory, J. C. Bean, R. Hull, and S. Nakahara, Phys. Rev. B **31**, 4063 (1985); D. Brasen, S. Nakahara, and J. C. Bean, J. Appl. Phys. **58**, 1860 (1985); J. C. Bean, T. T. Sheng, L. C. Feldman, A. T. Fiory, and R. T. Lynch, Appl. Phys. Lett. **44**, 102 (1984); F. Cerdeira, A. Pinczuk, and J. C. Bean, Phys. Rev. B **31**, 1202 (1985).

[8] T. P. Pearsall, F. H. Pollak, J. C. Bean, and R. Hull, Phys. Rev. B **33**, 6821 (1986).

[9] T. P. Pearsall, J. Bevk, L. C. Feldman, J. M. Bonar, J. P. Mannaerts, and A. Ourmazd, Phys. Rev. Lett. **58**, 729 (1987).

[10] T. P. Pearsall, J. Bevk, L. C. Feldman, J. M. Bonar, J. P. Mannaerts, and A. Ourmazd, J. Vac. Sci. Technol. B **15**, 1274 (1987); J. Bevk, J. P. Mannaerts, L. C. Feldman, B. A. Davison, and A. Ourmazd, Appl. Phys. Lett. **49**, 286 (1986); J. Bevk, A. Ourmazd, L. C. Feldman, T. P. Pearsall, J. M. Bonar, B. A. Davison, and J. P. Mannaerts, *ibid.* **50**, 760 (1987).

[11] T. Soma, Phys. Status Solidi B **95**, 427 (1979); M. Podgorny, G. Wolfgarten, and J. Pollmann, J. Phys. C **19**, L141 (1986); S. Krishnamurthy, A. Sher, and A. B. Chen, Phys. Rev. B **33**, 1026 (1986); M. Z. Huang and W. Y. Ching, Superlatt. Microstruct. **1**, 137 (1985).

[12] I. Morrison, M. Jaros, and K. B. Wong, J. Phys. C **19**, L239 (1986); J. Morrison and M. Jaros, Superlatt. Microstruct. **2**, 329 (1986).

[13] C. M. de Sterke and D. G. Hall, Phys. Rev. B **35**, 1380 (1987).

[14] U. Gnutzmann and K. Clausecker, Appl. Phys. **3**, 9 (1974).

[15] J. A. Moriarty and S. Krishnamurthy, J. Appl. Phys. **54**, 1892 (1983).

[16] C. G. Van de Walle and R. M. Martin, Phys. Rev. B **34**, 5621 (1986).

[17] S. Froyen, D. M. Wood, and A. Zunger, Phys. Rev. B **36**, 4547 (1987); S. Froyen, D. M. Wood, and A. Zunger, Mater. Res. Soc. Symp. Proc. **91**, 293 (1987).

[18] R. People and S. A. Jackson, Phys. Rev. B **36**, 1310 (1987); S. A. Jackson and R. People, Mater. Res. Soc. Symp. Proc. **56**, 365 (1986).

[19] L. Brey and C. Tejedor, Phys. Rev. Lett. **59**, 1022 (1987). Note that their Fig. 4 is mislabeled. The label C_1 in the lower part should read C_2.

[20] J. Ihm, A. Zunger, and M. L. Cohen, J. Phys. C **12**, 4409 (1979).

[21] O. H. Nielsen and R. M. Martin, Phys. Rev. B **32**, 3780 (1985).

[22] G. Kerker, J. Phys. C **13**, L189 (1980).

[23] P. Hohenberg and W. Kohn, Phys. Rev. **136**, 864 (1964); W.

Kohn and L. J. Sham, *ibid.* **140**, A1133 (1965).
[24]J. P. Perdew and A. Zunger, Phys. Rev. B **23**, 5048 (1981), and references therein.
[25]J. W. Matthews and A. E. Blakeslee, J. Cryst. Growth **27**, 118 (1974); R. People and J. C. Bean, Appl. Phys. Lett. **47**, 322 (1985); B. W. Dodson and P. A. Taylor, *ibid.* **49**, 642 (1986).
[26]P. N. Keating, Phys. Rev. **145**, 637 (1966).
[27]In the stress calculation, the values were adjusted as described in S. Froyen and M. L. Cohen, J. Phys. C **19**, 2623 (1986).
[28](a) Lattice constants are from R. W. G. Wyckoff, *Crystal Structures,* 2nd ed. (Interscience, New York, 1963), Vol. 1, p. 26. (b) Interband transition energies and effective masses of Si and Ge are taken from M. Cardona, G. Harbecke, O. Madelung, and U. Rossler, in *Physics of Group IV Elements and III-V Compounds,* Vol. 17a of *Landolt-Börnstein: Numerical Data and Functional Relationships in Science and Technology,* edited by O. Madelung (Springer, New York, 1982), Group III.
[29]The interplanar spacing deviations could have been caused by an erroneous c/a ratio and a difference in spring constants between the different layers. We did verify that this was not the case by confirming our results at $c/a=1.02$ and 1.04.
[30]J. L. Martins and A. Zunger, Phys. Rev. Lett. **56**, 1400 (1986); J. Mater. Res. **1**, 523 (1986).
[31]L. Nordheim, Ann. Phys. (Leipzig) **9**, 607 (1931).
[32]T. Narusawa and W. M. Gibson, Phys. Rev. Lett. **47**, 1459 (1981).
[33]F. H. Pollak and M. Cardona, Phys. Rev. **172**, 816 (1968); L. D. Laude, F. M. Pollak, and M. Cardona, Phys. Rev. B **3**, 2623 (1971); M. Chandrasekhar and F. M. Follak, *ibid.* **15**, 2127 (1977).
[34]K. J. Chang, S. Froyen, and M. L. Cohen, Solid State Commun. **50**, 105 (1984).
[35]C. Herring and E. Vogt, Phys. Rev. **101**, 966 (1956).
[36]R. People, Phys. Rev. B **32**, 1405 (1985).
[37]J. C. Hensel and G. Feher, Phys. Rev. **129**, 1041 (1963).
[38]L. D. Landau and E. N. Lifshitz, *Quantum Mechanics,* 2nd ed. (Pergamon, New York, 1975), p. 65.
[39]R. People, J. C. Bean, D. V. Lang, A. M. Sergent, H. L. Störmer, K. W. Secht, R. T. Lynch, and K. Baldwin, Appl. Phys. Lett. **45**, 1231 (1984).
[40]T. Fukui and H. Saito, Jpn. J. Appl. Phys. **23**, L521 (1984); **24**, L774 (1985).
[41]A. Ishibashi, Y. Mori, M. Itabashi, and N. Watanabe, J. Appl. Phys. **58**, 2691 (1985).
[42]J. J. Hopfield, J. Phys. Chem. Solids **15**, 97 (1960).
[43](a) D. E. Aspnes, Phys. Rev. B **12**, 2297 (1975); (b) A. Daunois and D. E. Aspnes, *ibid.* **18**, 1824 (1978).
[44]T. Nakayama and H. Kamimura, J. Phys. Soc. Jpn. **54**, 4726 (1985); N. Hamada and S. Ohnishi, Superlatt. Microstruct. **3**, 301 (1987).

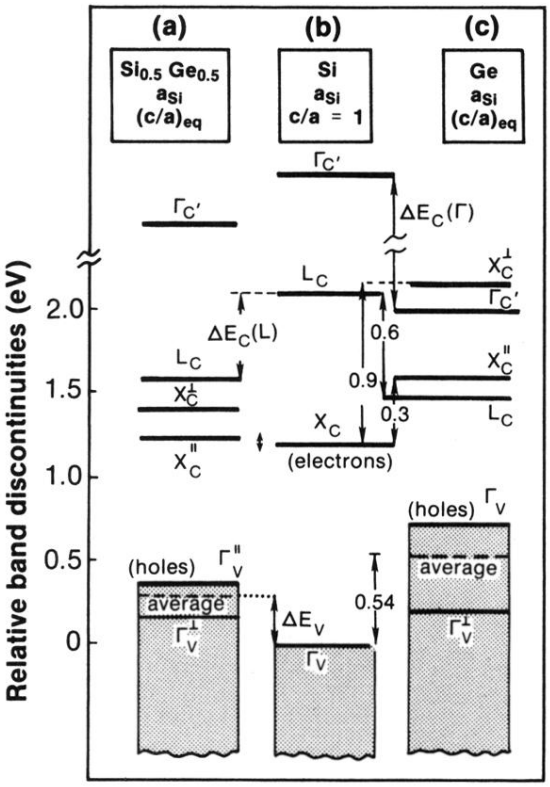

FIG. 2. Band-structure discontinuities of $Si_{0.5}Ge_{0.5}$/Si [(a) and (b)] and Ge/Si [(b) and (c)]. The valence-band offsets ΔE_v are taken from Ref. 16. Relative conduction-band offsets are obtained from Fig. 1, by positioning the average energy of $\Gamma_v^{\parallel}$ and $\Gamma_v^{\perp}$ (denoted "average") of one material at a distance ΔE_v from the average of the other material. Due to the LDA error, the magnitude of the gap cannot be reliably given. Shifting the conduction band upwards by ~ 0.6 eV (see text), however, produces realistic X, Δ, and L gaps.

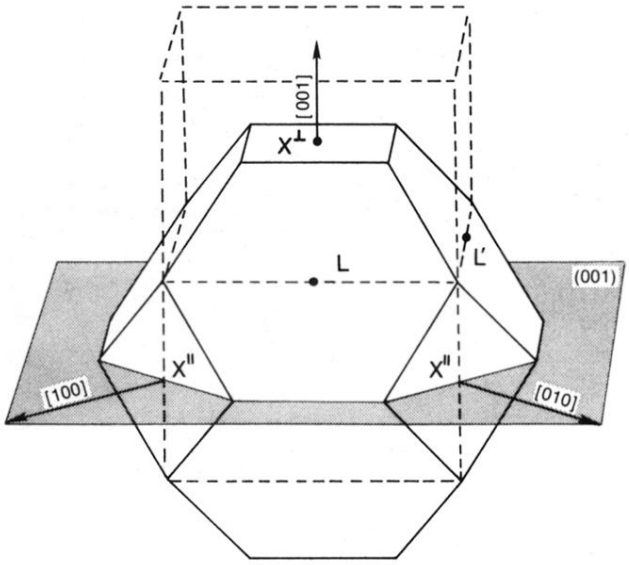

FIG. 3. Brillouin zone of the face-centered-cubic structure (solid lines) and the folded $n=2$ superlattice Brillouin zone (dashed lines), showing the nonfolding (L, $X^{\parallel}$, and L') as well as $\overline{\Gamma}$-folding ($X^{\perp}$) states.